Progress In Electromagnetics Research, Vol. 175, 149–157, 2022

Noninvasive Raman Imaging for Monitoring Mitochondrial Redox State in Septic Rats

Changwei Jiao[1, 2], Zijian Lin[1], Yinghe Xu[2], and Sailing He[2, 1, *]

Abstract—Raman imaging for a sepsis study is reported here. We propose a confocal resonance Raman microscopic imager (CRRMI) to measure in vivo the redox state of mitochondria over a surface area of a septic rat. The CRRMI has excellent performance with spectral and spatial resolutions of 0.1 nm and 2 µm, respectively. It is found that the Raman signal related to the mitochondrial dysfunction in sepsis is abnormally large only locally at many points with some random spatial distribution. Our CRRMI can detect the mitochondrial redox state through the skin of a naturally living rat even without the removal of hairs and overcomes some issues that a pointwise measurement method of Raman signals may encounter when monitoring mitochondrial dysfunction of a sepsis rat, such as the fluorescence of hairs, hitting the points without mitochondrial redox metabolic disorder, etc. The present Raman imager can be used for giving an early warning for sepsis. It provides a new method for noninvasive monitoring of mitochondrial redox state in sepsis.

1. INTRODUCTION

Sepsis is a fatal organ dysfunction syndrome caused by infection and host reaction disorder [1]. With an aging population, increased tumor incidence and increased invasive medical means, the incidence of sepsis is rising. It affects millions of people around the world every year and causes one-third to one sixth of deaths [2]. Sepsis has become a prominent public health problem, and it is also one of the major diseases that cause death in the world [3]. A study in 2020 shows that there are 48.9 million sepsis patients in the world, resulting in 11 million deaths per year, accounting for 19.7% of the total deaths, and the incidence rate is growing at a rate of 1.5%–9.0% every year [4]. The sequential organ failure assessment (SOFA) is adopted as the diagnostic standard of sepsis. However, SOFA is complicated in evaluation and requires a blood test, which is difficult to use quickly and may cause delay in diagnosis and treatment [5]. However, sepsis is likely to improve the prognosis if effective treatment measures are taken in the first few hours [6]. There is an urgent need to find a fast, simple, and continuous bedside detection method to identify sepsis accurately at an early stage, so as to achieve early diagnosis of sepsis, thereby reducing the mortality of sepsis patients with precise treatment.

The pathogenesis of mitochondrial damage caused by sepsis may involve a series of complex events [7–9]. Experimental evidence shows that mitochondrial dysfunction (including oxidative stress and energy metabolism) occurs at an early stage and is related to the outcome of sepsis [10, 11]. Sepsis-induced mitochondrial dysfunction or damage is a major cause of cellular metabolism disorder, and we use the redox state of mitochondria to measure the onset of sepsis in rats.

Resonance Raman scattering (RRS) uses a wavelength adjacent to the UV-visible absorption spectrum peak of the analyte as the excitation wavelength [12]. After absorbing the light, a molecule of the sample transits to a higher electron energy level and immediately returns to a vibrational level in the

Received 15 October 2022, Accepted 2 November 2022, Scheduled 10 November 2022
* Corresponding author: Sailing He (sailing@kth.se).
[1] Centre for Optical and Electromagnetic Research, National Engineering Research Center for Optical Instruments, Zhejiang University, Hangzhou 310058, China. [2] Taizhou Hospital, Zhejiang University, China.

ground state to generate resonance Raman scattering. RRS is a promising qualitative tool to analyze molecule vibrations and to identify molecular functions with structural fingerprints, even at negligibly low quantities [13–15]. Several studies have reported that RRS could be used to detect mitochondrial function in both isolated cells and tissues [16–19]. However, all these reported RRS results are based on pointwise (instead of imaging over an area) Raman spectroscopy measurement. In the present paper Raman imaging for a sepsis study is reported and the redox state of mitochondria is monitored over a gastrocnemius muscle surface area of a sepsis rat.

The spatial information of Raman spectral data on a rat gastrocnemius muscle surface is measured with a home-made confocal resonance Raman microscopic imager (CRRMI). Obtaining the Raman data over a surface area of a sepsis rat not only solves the problem of fluorescence generated by rat hairs at some points, but also reduces the probability of wrong data, particularly when we want to get the Raman signals from the subcutaneous gastrocnemius of a naturally living sepsis rat or human.

2. MATERIALS AND METHODS

2.1. Sample Preparation

In this study all adult male rats were obtained from the Animal Center of Taizhou Hospital (Zhejiang, China). Rats were housed in pathogen-free cages under standardized conditions with a 12-hour light/dark cycle (lights on from 8:00 am to 8:00 pm) and free access to food and water. All animal experiments were approved by the Animal Care and Use Committee at Taizhou Hospital (Zhejiang, China).

Cecal ligation and puncture (CLP) was performed as previously described in, e.g., [20]. Briefly, laparotomy was performed after the rats were anesthetized, and the cecum was gently exteriorized. Approximately 50% of the cecum was ligated with a 4-0 silk suture and double-punctured with a 21-gauge needle. A small amount (droplet) of feces was extruded from the surface of the cecum, and the peritoneum was closed. Then, the rats were resuscitated via subcutaneous injection of prewarmed 0.9% normal saline (5 ml/100 g) and placed on a temperature controlled pad until they regained independent mobility. Survival was continuously monitored for up to 7 days.

We have carried out the above CLP operations for four rats (sepsis group), and sham operation (pseudo-surgery: only Cecal ligation but no puncture) for three other rats (the pseudo-surgery group).

2.2. System Setup

In the present paper we use a home-made confocal resonance Raman microscopic imager (CRRMI). The confocal feature can help us filter out the interference information (especially the interference information in the Z-axis direction) the nonfocus area, and a high signal-to-noise ratio can be achieved. Through galvanometer scanning, we can obtain the Raman image, which includes the spatial distribution information of the sample and the corresponding Raman signal at each point. Combining these two kinds of information, our CRRMI can play an excellent role in sample identification and classification.

Our home-made CRRMI has an excellent optical performance, in which the spectral resolution reaches 0.1 nm and the spatial resolution reaches 2 μm. The optical path diagram and schematic of our CRRMI are shown in Figures 1(a) and (b), respectively. A 532 nm fiber laser (MGL-FN-532, Changchun) is utilized as the excitation light. For the excitation light, the spot quality factor $M \wedge 2$ is less than 1.1, the spot mode is TEM00, the working mode is continuous wave, and the output power is adjustable in the range of $0 \sim 100$ mw. The laser is coupled into the optical system through a collimator, a reflector (GCC10220, Daheng Optics, China) and a beam splitter (BS1). The light then enters the galvanometer system with the angle of the incident light adjusted by controlling the galvanometer angle, so that the excitation light shines at different points of the sample to achieve the effect of point scanning. The scanning lens and telecentric lens (ITL200) are used to optimize the scanning image plane and adjust the spot diameter. This way the excitation light from different angles can always converge on the incident pupil of the microscope objective after passing through the reflector. The sample is always at the best focal plane of the system by using a motorized positioning system to control the distance between the objective lens and the sample. The sample points irradiated by the laser generate Raman signals. After being collimated by the microscope objective lens, the Raman signals will return along the original

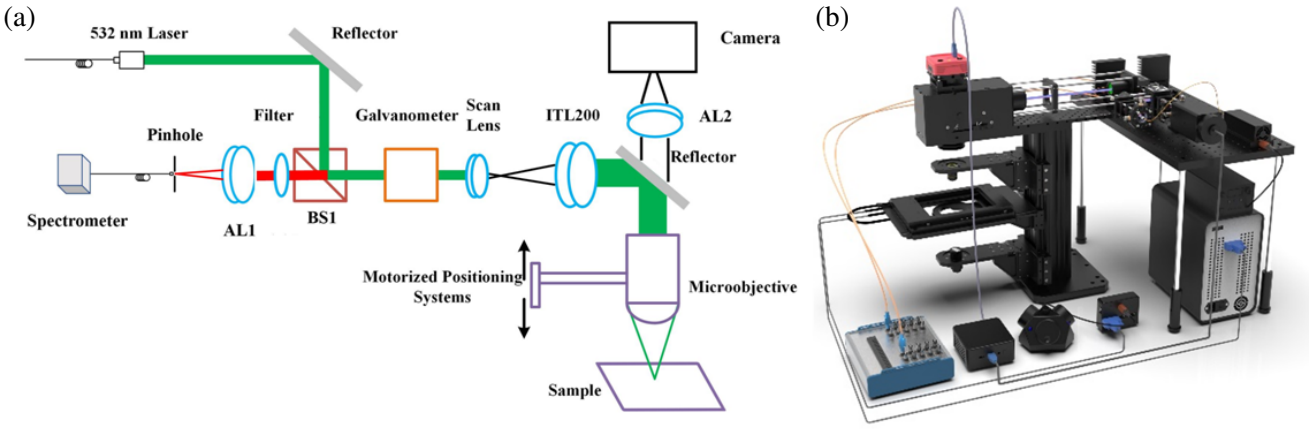

Figure 1. Optical path diagram and physical diagram of CRRMI.

optical path, passing through the reflector, telecentric lens (ITL200), scanning lens, galvanometer and beam splitter (BS-1), and reaching the receiver at the rear end, which is connected to a spectrometer with 0.1 nm spectral resolution.

A 532 nm notch filter is used to filter out the excitation light, so that the excitation light and the Raman signal of the sample can be separated. Then, the obtained Raman signal is focused on the pinhole through the achromatic lens (AL-1, Daheng Optics, China). The pinhole structure only allows the Raman signal generated at the sampling point where the excitation light is focused to pass through, while the signal generated at other locations is blocked. The confocal optical path formed in this way can eliminate the interference of axial or adjacent Raman signals, so that the signal-to-noise ratio can be greatly improved. By changing the angle of the excitation light using the galvanometer, the Raman signals excited at different points of the sample will pass through the pinhole in turn to form a complete Raman image.

In order to test the spatial resolution, we used a standard resolution test plate with a final resolution of 2 µm to conduct imaging experiments. The objective lens of 10x magnification microscope (OLYMPUS Inc., LUMPLFLW series) is utilized. The image results shown in Figure 2 indicate that the spatial resolution of our system is better than 2 µm as the minimum resolution mode can be clearly seen.

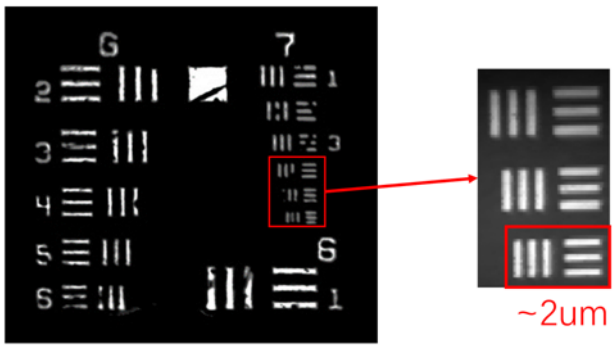

Figure 2. The Raman images captured by the CRRMI have a high signal-to-noise ratio.

Figure 3. A rat on the platform of the CRRMI system for Raman imaging.

As shown in Figure 3, a rat was fixed on the stage after being anesthetized. Then we take the Raman image of the rat gastrocnemius muscle in vivo by using our CRRMI system.

3. EXPERIMENTAL RESULTS AND DISCUSSIONS

The resonance Raman signals from the gastrocnemius muscle of sepsis rats at different times are shown in Figure 4, which shows that the resonance Raman signals (at the fixed characteristic wavenumber of 750 cm^{-1}, 1130 cm^{-1}, 1580 cm^{-1}, related to the molecule structures of symmetric vibrations of porphyrin, vibrations of Cb-CH3 side radicals and vibrations of methine bridges (CaCm, CaCmH bonds), as previously described [21, 22]) of the rat become abnormally large two hours after cecal puncture of the rats.

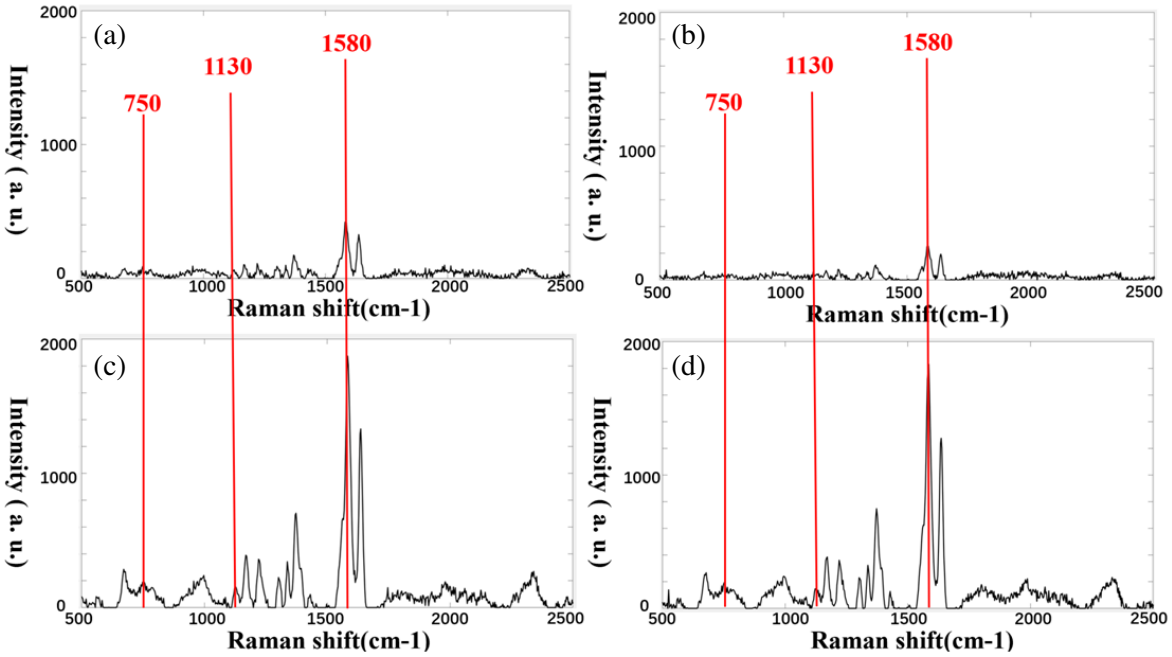

Figure 4. (a)–(d) The resonance Raman signal of gastrocnemius muscle in sepsis rats at 0, 1, 2, 3 hours (after the CPL), respectively.

In previous related work, pointwise Raman detection was used by other research groups. We have also tried to use pointwise Raman detection. However, since Raman spectra were detected at only one or several points of the rat surface, contingency and uncertainty occur often. For example, when the focused laser light hits some hairs of the rat, large fluorescence was generated (shown in Figure 5) and the useful Raman signal of mitochondrial will be submerged into large fluorescence (as noise).

Figures 6(a) and (c) show the resonance Raman imaging of live gastrocnemius muscle of a rat in the sham operation group at a fixed characteristic wavenumber of 1580 cm^{-1}, and clearly we see that the mitochondrial redox state of rats in this group is normal. When the rat's sepsis is not serious, the mitochondrial redox state is abnormally large only locally at many points with some random distribution, and our sampling point may just miss the abnormal points. As shown in Figure 6(b), there are also normal spots on sepsis rats (white spots shown in the figure). If the pointwise Raman detection just hits a position of normal spots, a false negative will be reported. The resonance Raman imaging we introduce in the present paper can simultaneously obtain the two-dimensional spatial distribution of the resonance Raman spectrum over an area of the rat surface, and thus can avoid the problems encountered in the pointwise Raman detection. The present Raman imaging method allows for the early detection of mitochondrial redox disorder.

In order to verify the above statement by removing the possible disturbance due to the small movement of the live rat (though anesthetized) in our experiment, we cut off a gastrocnemius muscle of a rat and performed again the confocal resonance Raman imaging, as shown in Figure 7. For the cut-off gastrocnemius muscle from the sepsis rat, the mitochondrial redox state is abnormally large only locally at many points with some random distribution.

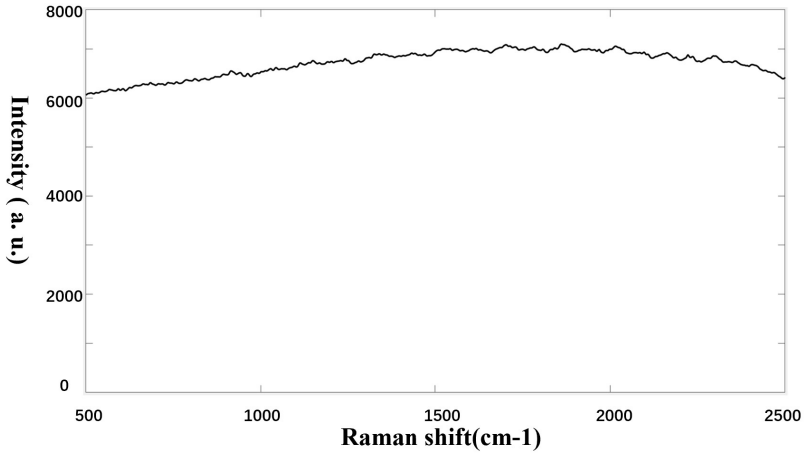

Figure 5. The large fluorescence (detected by the pointwise Raman spectrometer) generated by a hair of the rat when the laser hits the hair. Our effective Raman signal is submerged into large fluorescence (as noise).

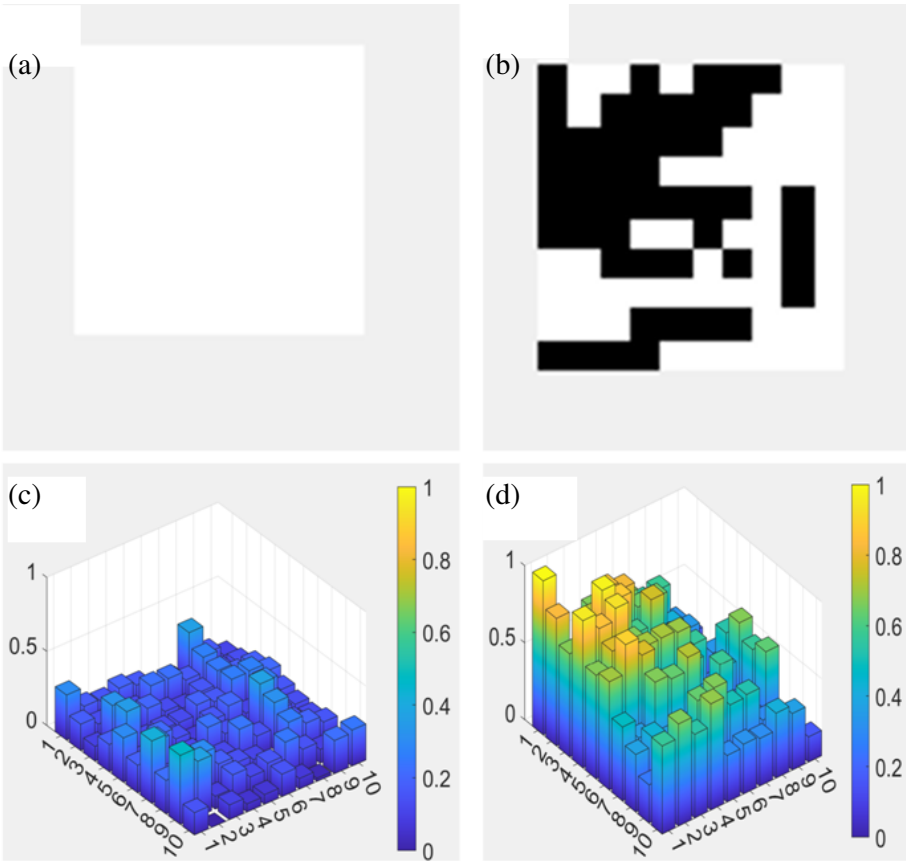

Figure 6. (a) and (c) are the Raman spectral imaging (at the fixed characteristic wavenumber of $1580\,\mathrm{cm}^{-1}$) of live gastrocnemius muscle of a rat in the sham operation group, and (b) and (d) are the Raman spectral imaging of live gastrocnemius muscle of a rat with sepsis. A white point is a healthy location identified by the threshold algorithm, and a black point is a location with mitochondrial damage identified by the threshold algorithm. It is obvious that Raman imaging can avoid the issue of the large fluorescence influence from a hair.

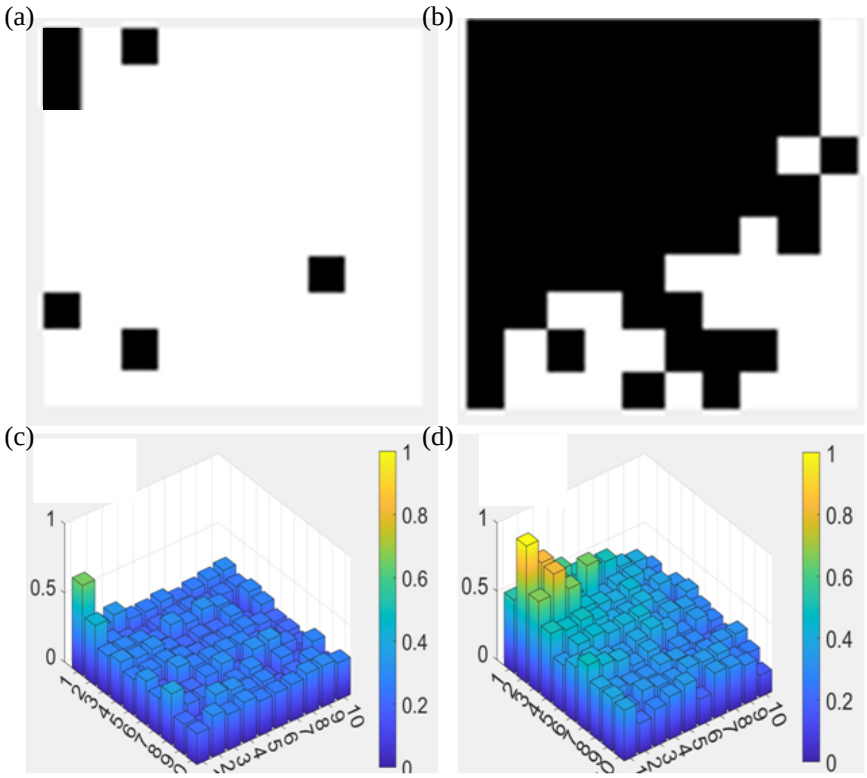

Figure 7. The Raman spectral imaging of ex-vivo gastrocnemius muscle of a rat in the sham operation group ((a) and (c)), and a rat with sepsis ((b) and (d)).

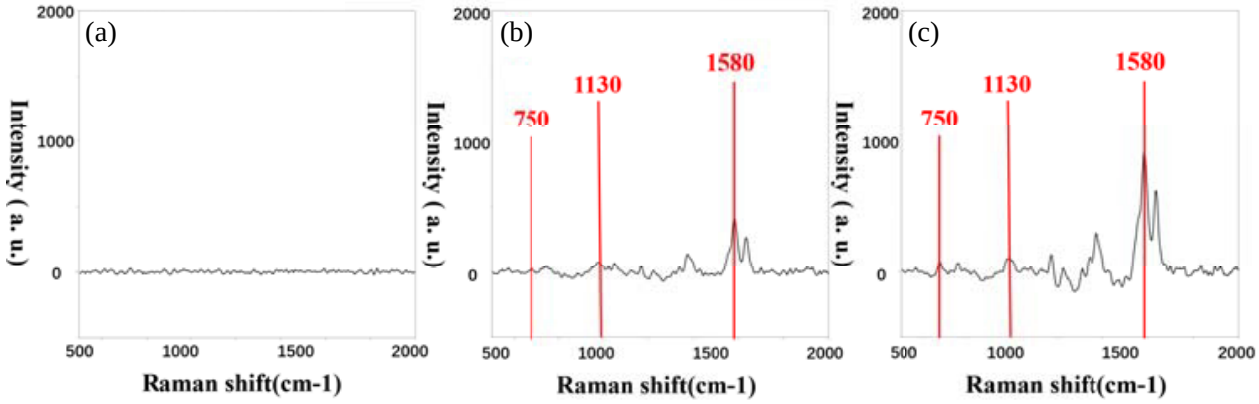

Figure 8. (a) The Raman signal of serum in a sepsis rat at the fifth hour (after the injection). (b), (c) The Raman signals of blood cells in a sepsis rat at the fifth and fifteenth hours (after the injection), respectively.

Mitochondria also exist in blood. Here we also use CRRMI to detect the redox state of mitochondria in blood cells of septic rats. First, sepsis was induced to the rats by injecting polysaccharide. Then blood was collected from rats at regular intervals. After the obtained blood was centrifugated (4°, 3000 RPM, 10 minutes), separated rat serum and blood cells were obtained. Figure 8 shows the Raman signals (averaged over 5 neighboring points) measured with our CRRMI system. The Raman signal of serum (Figure 8(a)) is very weak as compared to that of blood cells (Figure 8(b)) from a septic rat. Note that the Raman signals from both serum and blood cells are very weak for a rat in the sham operation group.

As shown in Figure 8, the Raman signals of blood cells of septic rats at $750\,\mathrm{cm}^{-1}$, $1130\,\mathrm{cm}^{-1}$, $1580\,\mathrm{cm}^{-1}$ show an increasing trend over the time, and these Raman signals in blood cells are related to the redox state of mitochondria. The measurement results indicate the potential of our CRRMI in monitoring the mitochondrial redox state of blood cells for early warning of sepsis.

Our CRRMI has the advantage of detecting the mitochondrial redox state through the skin (i.e., a naturally living rat without removal of hairs), as shown in Figure 9. As expected, as compared with the large resonance Raman signal from the exposed gastrocnemius of the sepsis rat (shown in Figure 9(b)), the resonance Raman signal of the sepsis rat detected through the skin (shown in Figure 9(a)) is a bit smaller, but still clearly observable.

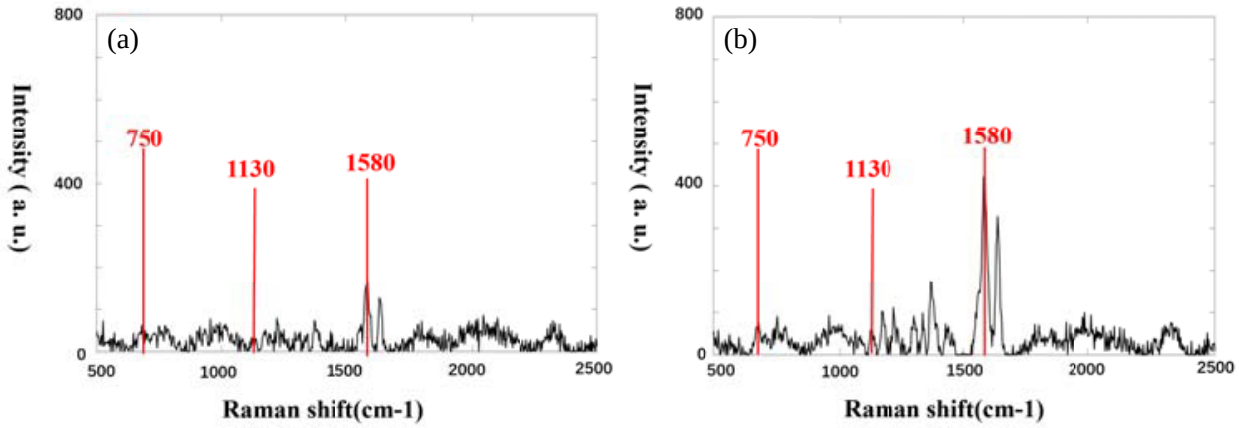

Figure 9. (a) shows the Raman signal detected through the skin of a sepsis rat, and (b) shows the signal directly detected from an exposed gastrocnemius of a sepsis rat.

From Figure 9 we can see that the presence of skin will weaken our detected Raman signal and reduce the signal-to-noise ratio. However, the effective signal is still clearly measurable. Therefore, it is possible to realize non-invasive detection of sepsis with our confocal resonance Raman microscopic imager.

4. SUMMARY AND OUTLOOK

In the present work, we have proposed a confocal resonance Raman microscopic imager (CRRMI) for the detection of sepsis in rats. Our Raman imaging instrument can measure the spatial distribution of Raman spectrum over a certain surface area of the sample, and the amount of the collected data is sufficient to overcome some issues that a pointwise measurement method for Raman signals may encounter when measuring a sepsis rat, such as the fluorescence of hairs, the laser hitting the points without mitochondrial dysfunction, etc. The results presented in this paper are generally valid for different rats we have measured, through the imaging data are shown for simplicity only for a specific rat as a representative case. Further studies will be aimed at increasing the detection speed, wavelength range and portability [26, 27]. It is possible to combine the CRRMI system with snapshot Raman imaging technology [23], which would eliminate the need to scan, thus improving the detection speed and reducing the cost. What's more, our system can be combined with fluorescence spectrum and other means to make our system more versatile [28, 29]. Furthermore, combined with 3D imaging method [24, 25], the system could realize 4D (1D in spectral and 3D in spatial) detection, for multi-dimensional and more comprehensive inspection applications.

FUNDING

This work was supported by Key Research and Development Program of Zhejiang Province (2022C03051), Zhejiang Provincial Natural Science Foundation of China under Grant No. LY20H150008,

the National Natural Science Foundation of China (No. 11621101), and the National Key Research and Development Program of China (No. 2018YFC1407503).

ACKNOWLEDGMENT

We appreciate Yongpo Jiang, Xiong Tian and Xiaoxiao Zhao of Taizhou Hospital, and Jin Luo and Julian Evans of COER@Zhejiang University for valuable helps.

DISCLOSURES

The authors declare no conflicts of interest.

REFERENCES

1. Singer, M., C. S. Deutschman, C. W. Seymour, et al., "The third international consensus definitions for sepsis and septic shock (Sepsis-3)," *JAMA*, Vol. 315, 801–810, 2016.
2. Evans, L., A. Rhodes, W. Alhazzani, et al., "Surviving sepsis campaign: International guidelines for management of sepsis and septic shock 2021," *Intensive Care Med.*, Vol. 47, 1181–1247, 2021.
3. Rudd, K. E., S. C. Johnson, K. M. Agesa, et al., "Global, regional, and national sepsis incidence and mortality, 1990–2017: Analysis for the global burden of disease study," *Lancet*, Vol. 395, 200–211, 2020.
4. Cecconi, M., L. Evans, M. Levy, et al., "Sepsis and septic shock," *Lancet*, Vol. 392, 75–87, 2018.
5. Liu, V. X., Y. Lu, K. A. Carey, E. R. Gilbert, M. Afshar, M. Akel, N. S. Shah, J. Dolan, C. Winslow, P. Kipnis, D. P. Edelson, G. J. Escobar, and M. M. Churpek, "Comparison of early warning scoring systems for hospitalized patients with and without infection at risk for in-hospital mortality and transfer to the intensive care unit," *JAMA Netw. Open*, Vol. 3, e205191, 2020.
6. Reinhart, K., R. Daniels, N. Kissoon, F. R. Machado, R. D. Schachter, and S. Finfer, "Recognizing sepsis as a global health priority — A WHO resolution," *N. Engl. J. Med.*, Vol. 377, 414–417, 2017.
7. Singer, M., "The role of mitochondrial dysfunction in sepsis-induced multi-organ failure," *Virulence*, Vol. 5, 66–72, 2014.
8. Fink, M. P., "Cytopathic hypoxia, is oxygen use impaired in sepsis as a result of an acquired intrinsic derangement in cellular respiration?," *Crit. Care Clin.*, Vol. 18, 165–175, 2002.
9. Galley, H. F., "Oxidative stress and mitochondrial dysfunction in sepsis," *Br. J. Anaesth.*, Vol. 107, 57–64, 2011.
10. Crouser, E. D., M. W. Julian, J. E. Huff, J. Struck, and C. H. Cook, "Carbamoyl phosphate synthase-1: A marker of mitochondrial damage and depletion in the liver during sepsis," *Crit. Care Med.*, Vol. 34, 2439–2446, 2006.
11. Carré, J. E., J.-C. Orban, L. Re, K. Felsmann, W. Iffert, M. Bauer, H. B. Suliman, C. A. Piantadosi, T. M. Mayhew, P. Breen, M. Stotz, and M. Singer, "Survival in critical illness is associated with early activation of mitochondrial biogenesis," *Am. J. Respir Crit. Care Med.*, Vol. 182, 745–751, 2010.
12. Robert, B., "Resonance Raman spectroscopy," *Photosynthesis Research*, Vol. 101, 147–155, 2009.
13. Spiro, T. G., "Resonance Raman spectroscopy. New structure probe for biological chromophores," *Acc. Chem. Res.*, Vol. 7, 339–344, 1974.
14. Spiro, T. G. and T. C. Strekas, "Resonance Raman spectra of hemoglobin and cytochrome c: Inverse polarization and vibronic scattering," *Proc. Natl. Acad. Sci.*, Vol. 69, 2622–2626, USA, 1972.
15. Perry, D. A., J. W. Salvin, P. Romfh, P. L. Chen, K. Krishnamurthy, L. M. Thomson, B. D. Polizzotti, F. X. McGowan, D. Vakhshoori, and J. N. Kheir, "Responsive monitoring of mitochondrial redox states in heart muscle predicts impending cardiac arrest," *Sci. Transl. Med.*, Vol. 9, eaan0117, 2017.

16. Carré, J. E., J.-C. Orban, L. Re, K. Felsmann, W. Iffert, M. Bauer, H. B. Suliman, C. A. Piantadosi, T. M. Mayhew, P. Breen, M. Stotz, and M. Singer, "Survival in critical illness is associated with early activation of mitochondrial biogenesis," *Am. J. Respir Crit. Care Med.*, Vol. 182, 745–751, 2010.
17. Lalonde, J. W., G. D. Noojin, N. J. Pope, S. M. Powell, V. V. Yakovlev, and M. L. Denton, "Continuous assessment of metabolic activity of mitochondria using resonance Raman microspectroscopy," *Journal of Biophotonics*, Vol. 14, e202000384, 2021.
18. Morimoto, T., L. D. Chiu, H. Kanda, H. Kawagoe, T. Ozawa, M. Nakamura, K. Nishida, K. Fujita, and T. Fujikado, "Using redox-sensitive mitochondrial cytochrome Raman bands for label-free detection of mitochondrial dysfunction," *Analyst*, Vol. 144, 2531–2540, 2019.
19. Brazhe, N. A., M. Treiman, B. Faricelli, J. H. Vestergaard, and O. Sosnovtseva, "In situ Raman study of redox state changes of mitochondrial cytochromes in a perfused rat heart," *PLoS One*, Vol. 8, e70488, 2013.
20. Rittirsch, D., M. S. Huber-Lang, M. A. Flierl, and P. A. Ward, "Immunodesign of experimental sepsis by cecal ligation and puncture," *Nat. Protoc.*, Vol. 4, 31–36, 2009.
21. Brazhe, N. A., M. Treiman, A. R. Brazhe, N. L. Find, G. V. Maksimov, and O. V. Sosnovtseva, "Mapping of redox state of mitochondrial cytochromes in live cardiomyocytes using Raman microspectroscopy," *PLoS One*, Vol. 7, e41990, 2012.
22. Chen, Z., J. Liu, L. Tian, Q. Zhang, Y. Guan, L. Chen, G. Liu, H.-Q. Yu, Y. Tian, and Q. Huang, "Raman micro-spectroscopy monitoring of cytochrome c redox state in Candida utilis during cell death under low-temperature plasma-induced oxidative stress," *Analyst*, Vol. 145, 2020.
23. Brückner, M., K. Becker, J. Popp, and T. Frosch, "Fiber array based hyperspectral Raman imaging for chemical selective analysis of malaria-infected red blood cells," *Analytica Chimica Acta*, Vol. 894, 76–84, 2015.
24. Luo, J., S. Li, E. Forsberg, and S. He, "4D surface shape measurement system with high spectral resolution and great depth accuracy," *OE*, Vol. 29, 13048–13070, 2021.
25. Luo, J., Z. Lin, Y. Xing, E. Forsberg, C. Wu, X. Zhu, T. Guo, G. Wang, B. Bian, D. Wu, and S. He, "Portable 4D snapshot hyperspectral imager for fast spectral and surface morphology measurements," *Progress In Electromagnetics Research*, Vol. 173, 25–36, 2022.
26. Li, J., F. Cai, Y. Dong, Z. Zhu, X. Sun, H. Zhang, and S. He, "A portable confocal hyperspectral microscope without any scan or tube lens and its application in fluorescence and Raman spectral imaging," *Optics Communications*, Vol. 392, 1–6, 2017.
27. Shen, F., H. Deng, L. Yu, and F. Cai, "Open-source mobile multispectral imaging system and its applications in biological sample sensing," *Spectrochimica Acta, Part A: Molecular and Biomolecular Spectroscopy*, Vol. 280, 121504, 2022.
28. Xu, Z., Y. Jiang, J. Ji, E. Forsberg, Y. Li, and S. He, "Classification, identification, and growth stage estimation of microalgae based on transmission hyperspectral microscopic imaging and machine learning," *OE*, Vol. 28, 30686, 2020.
29. Xu, Z., Y. Jiang, and S. He, "Multi-mode microscopic hyperspectral imager for the sensing of biological samples," *Applied Sciences*, Vol. 10, 4876, 2020.